

Shock Response of Commercial Purity Polycrystalline Magnesium Under Uniaxial Strain at Elevated Temperatures

Tianxue Wang¹ · Bryan Zuanetti¹ · Vikas Prakash¹

Received: 7 May 2017 / Accepted: 1 September 2017 / Published online: 7 September 2017
© Society for Experimental Mechanics, Inc 2017

Abstract In the present paper, results of plate impact experiments designed to investigate the onset of incipient plasticity in commercial purity polycrystalline magnesium (99.9%) under weak uniaxial strain compression and elevated temperatures up to melt are presented. The dynamic stress at yield and post yield of magnesium, as inferred from the measured normal component of the particle velocity histories at the free (rear) surface of the target plate, are observed to decrease progressively with increasing test temperatures in the range from 23 to 500 °C. At (higher) test temperatures in the range 500–610 °C, the rate of decrease of dynamic stress with temperature at yield and post-yield in the sample is observed to weaken. At still higher test temperatures (617 and 630 °C), a dramatic increase in dynamic yield as well as flow stress is observed indicating a change in dominant mechanism of plastic deformation as the sample approaches the melt point of magnesium at strain rates of $\sim 10^5$ /s. In addition to these measurements at the wavefront, the plateau region of the free surface particle velocity profiles indicates that the longitudinal (plastic) impedance of the magnesium samples decreases continuously as the sample temperatures are increased from room to 610 °C, and then reverses trend (indicating increasing material longitudinal impedance/strength) as the sample temperatures are increased to 617 and 630 °C. Electron back scattered diffraction analysis of the as-received and annealed pre-test magnesium samples reveal grain coarsening as well as grain re-orientation to a different texture during the heating process of the samples.

Keywords Commercial purity polycrystalline magnesium · Elevated temperature plate impact experiments · Incipient plasticity · Dynamic yield and flow stress · Near-melt temperatures · Ultra-high strain rates

Introduction

Hexagonal close-packed (HCP) materials have seen increasing use in structural applications. This has mainly been owing to their high specific strength relative to traditional structural materials. This increased usage has led to a surge in research and development activities in the area of HCP materials for structural applications. As a result, the previous deficit in understanding of the mechanical behavior of HCP materials relative to face-centered cubic (FCC) and body-centered cubic (BCC) materials has been drastically improved over the past 10 years [1, 2]. Despite these advances in our understanding, significant questions still remain—in particular with regards to how hcp materials behave under high strain-rate loading.

In general, at room temperature, plastic deformation in HCP lattice structure is accommodated by easy glide of dislocations along the basal, prismatic and pyramidal planes in the $\langle 1\ 1\ \bar{2}\ 0 \rangle$ directions, commonly referred to as $\langle a \rangle$ type slip systems. Owing to the three easily activated $\langle a \rangle$ type slip systems having the same slip direction, they reduce to only four independent slip systems. However, to accommodate compatible plastic strains in a polycrystalline metal, a total of five independent slip systems are required [3, 4]. Thus, to meet the criteria for compatible plastic strains, a further non $\langle a \rangle$ type slip system must be activated. Typically, this is accommodated by a so-called $\langle c + a \rangle$ type (pyramidal) slip system.

✉ Vikas Prakash
vikas.prakash@case.edu

¹ Department of Mechanical and Aerospace Engineering, Case Western Reserve University, Cleveland, OH 44106-7222, USA

The critically resolved shear stress (CRSS) required to activate the different slip systems in magnesium, varies significantly depending on the temperature and composition. Generally, the CRSS for the $\langle c + a \rangle$ type slip system is higher than that of the $\langle a \rangle$ type slip systems, leading to anisotropic plastic deformation behavior at the single-crystal level. The CRSS of basal slip has been observed to be nearly independent of the temperature [5]. On the contrary, the CRSS of prismatic and pyramidal slip decreases with the increasing temperature. Thus, at elevated temperatures, enhanced activity of pyramidal $\langle c + a \rangle$ slip is expected to accommodate the plastic deformation along the c -axis [6]. Also, it is well established that increasing the strain rate increases the CRSS by decreasing the time for a given dislocation to overcome a barrier to its motion. At extremely high strain rates, the glide of dislocations is further inhibited by mechanisms such as phonon drag [7, 8].

It has been argued that incompatible plastic strains in polycrystalline HCP metals can also be accommodated by the activation of deformation twinning. Deformation twinning results in a reorientation of the crystal lattice around a given plane and in a given direction. This reorientation accommodates plastic strain and, more importantly, typically re-orientates the crystal lattice for easier crystallographic slip. The most commonly observed twinning modes in magnesium are $\{10\bar{1}2\} < \bar{1}011 >$ extension twinning and $\{10\bar{1}1\} < 10\bar{1}\bar{2} >$ contraction twinning, which sometimes are also referred as tensile twinning and compression twinning, respectively. It is generally accepted that $\{10\bar{1}2\} < \bar{1}011 >$ extension twinning is the most easily activated twin system in magnesium. Deformation twinning is particularly important at high strain rates, where it has been observed that twinning becomes more prevalent.

Several studies regarding strain-rate dependence of flow stress of pure magnesium at room temperature have been published over the last decade. For example, magnesium single crystal samples loaded at room temperature under compression at about 10° from the c -axis under quasi-static ($\sim 10^{-3}$ /s) and intermediate strain-rates (10^2 – 10^3 /s), have revealed a high sensitivity of mechanical strength and hardening to strain-rates [9]. On the contrary, similar studies performed on specimens loaded perpendicular to the c -axis of most grains, have shown a lack of sensitivity to strain-rate [10]. These results are a few among many which demonstrate the sensitivity of the mechanical strength and rate-dependent behavior of magnesium to varying texture. The rate dependencies of the flow stress of magnesium and magnesium alloys with different textures are summarized in [11] at strain-rates ranging from 10^{-4} to 10^3 /s. High sensitivity of flow stress to strain-rate is observed when plastic flow is accommodated by dislocation slip, and contrariwise when plastic flow is accommodated by extension twinning.

The temperature dependence of the mechanical strength of magnesium has also been investigated by several researchers [12–14]. Experiments performed on high purity single crystal magnesium loaded in tension perpendicular to the c -axis at temperatures ranging from 23 to 450 °C and strain-rates in the range 2.3×10^{-3} – 2.3×10^{-1} /s, have shown remarkable thermal softening [12]. Microstructural studies of the post-test specimens indicate plastic deformation to be accommodated primarily by non-basal slip systems [12]. Similarly, pure magnesium single crystals subjected to plane-strain compression along the c -axis at a constant strain rate of 10^{-3} /s and at temperatures ranging from 200 to 370 °C also showed a decrease in material strength with increasing temperatures [13]. More recently, annealed pure magnesium single crystals were shock-loaded along directions parallel to and at 45° to the c -axis at temperatures ranging from 20 to 503 °C and strain rates in the range 10^4 – 10^6 /s [14]. In these experiments, an increase in the dynamic yield stress under uniaxial strain compression, inferred from free surface particle velocities at the Hugoniot elastic limit (HEL), was observed with increasing temperatures along both the c -axis and at 45° to c -axis. Even though, there is no consensus to explain the mechanism of the increase in the dynamic stress at HEL of magnesium, similar studies on pure polycrystalline cobalt, which also displays an hcp crystal structure, indicate that the growth in dynamic stress at HEL with temperature (in magnesium and cobalt) may be controlled by phonon drag [15]. However, similar growth in dynamic flow stress with temperature was not observed in zinc single crystal (another hcp metal), when impacted on the prismatic plane [14], suggesting that strengthening effects induced by phonon drag may not be dominant when extension twinning is highly favored.

The motivation for the present series of experiments is driven by the critical need for experimental data on commercial purity polycrystalline magnesium at ultra-high loading rates and elevated temperatures up to the melt point of magnesium, which can aid in providing a better understanding of the dominant deformation mechanisms in polycrystalline magnesium under extreme thermo-mechanical loading conditions. In order to conduct these experiments, the recently developed elevated-temperature reverse geometry plate impact configuration is utilized, where a heated flyer carried by a custom designed heat-resistant sabot is made to impact a stationary target plate. A description of the experimental approach employed in the present experiments is provided in “[Experimental Work](#)”. “[Experimental Results and Discussion](#)” provides the experimental results on the temperature dependence of the dynamic yield stress under uniaxial strain compression and the dynamic flow stress post yield of commercial purity magnesium (99.9%) under shock compression at temperatures ranging from 23 to 630 °C, along with the effects of micro-structural changes due to coarsening of the

grain size and texture development on the measured dynamic mechanical response. The key points of the present study are summarized in "Summary".

Experimental Work

Flyer (Sample) and Target Materials

For the experiments conducted in the present study, a 99.9% commercial purity polycrystalline magnesium rod having a diameter of 76 mm was procured from Goodfellow Corporation. Select physical properties of the polycrystalline magnesium are shown in Table 1. Sample disks of diameter 76 mm and thickness 5.6 mm were machined from the as-received rod. In order to achieve the flatness tolerance of the sample disks, they were ground flat to within 12 μm and then lapped to within 2–3 Newton’s rings across the sample diameter. The flatness was ensured using a λ/10 optical flat placed in contact with the polished sample surface under a green monochromatic light source [16].

The microstructure of the as-received magnesium was examined using electron backscatter diffraction (EBSD) analysis in the extrusion direction (ED) of the rod (thickness direction of the sample). The [0001] and [10 $\bar{1}$ 0] poles of the hcp crystal along with the extrusion and radial directions of the pure magnesium rod are shown in Fig. 1a. The normal to the {10 $\bar{1}$ 0} planes are parallel to the impact direction (extrusion direction) while the normal to the {0001} planes (c-axis) lies parallel to the radial direction of the magnesium rod. The initial grain size and the texture of the as-received samples are demonstrated by the grain orientation map and the pole figure shown in Fig. 1b, c respectively. A weighted average grain size of ~77 μm is inferred for the as-received material from the EBSD data.

Similar microstructural characterization was performed on the annealed samples heated for at least 0.5 h at 600 °C and then allowed to cool slowly in vacuum. From the EBSD grain orientation map (Fig. 2a), extensive grain coarsening is revealed. The weighted average grain size is ~547 μm, which is much larger when compared to the grain size in the as-received material. Additionally, development of a texture is observed as a consequence of the [0001] basal poles reorienting closer towards the extrusion direction (ED) after annealing (Fig. 2b).

The target material assembly consists of a precipitation hardened Inconel 718 disk (~25 mm in diameter and ~7 mm in thickness), adhered to a precision machined aluminum ring with outer and inner diameters of 41 and 32 mm, respectively. The target assembly is housed within a larger diameter Delrin ring, which is bolted securely to a target holder. The Inconel target disks are machined from a 25.4 mm diameter precipitation hardened Inconel 718 rod procured from High Temp Metals Inc. Select physical properties of Inconel 718 are shown in Table 2. The aluminum ring comprises of six equi-spaced 1.5 mm radial slots housing six copper pins with non-conductive epoxy on a bolt circle of diameter 34.5 mm. The copper pins are lapped flush to the target surface to within 2–3 Newton’s rings across the target diameter. Prior to adhering the target components together, the rear surface of the Inconel 718 disk is polished using 1 μm diamond polishing paste to enable laser interferometry measurements [17–20]. The dimensions of the flyer and the target plates provide a window time of ~1.3 μs before unloading waves arrive from the lateral boundary of the target plate at the monitoring point on the rear surface of the target plate [16].

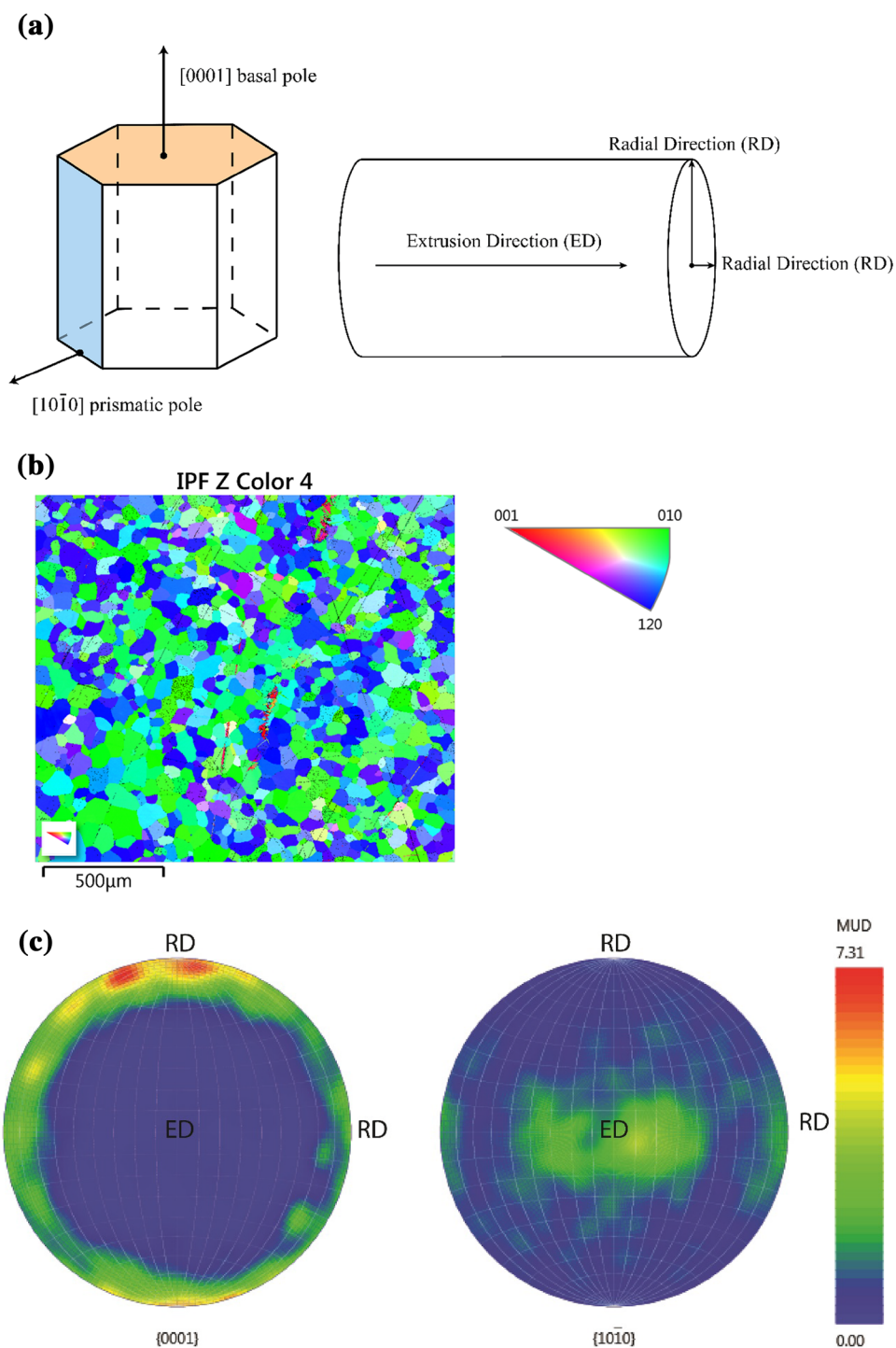
Elevated Temperature Normal Plate Impact Experiments

Previous experimental work on elevated temperature plate impact experiments have involved normal plate impact shock compression experiments [14, 15], where a resistive heater is utilized to heat the target (specimen), and elevated temperature combined pressure-and-shear plate impact experiments [21], where a thin foil metal sample is sandwiched between the front and back target plates and heated via an induction coil system at the target chamber end of the gas gun. Even though, the addition of the resistive or induction coil heating elements to the impact chamber of the gas-gun to heat the target disk have been shown to be feasible, it leads to several experimental challenges: first, heating the metal target (sample) using an induction coil heating system or a resistive heater, subjects various elements of the target holder and/or the alignment-fixture to differential thermal expansion, requiring remotely controlled alignment adjustment tools with continuing feedback for maintaining parallelism of the target and flyer plates; second, heating the target plate in combined pressure-shear plate impact configuration requires

Table 1 Select physical properties of 99.9% pure polycrystalline magnesium

Material	Density (Kg/m ³)	Elastic modulus (GPa)	Shear modulus (GPa)	Poisson’s ratio	Longitudinal wave speed (M/S)	Shear wave speed (m/s)
99.9% Polycrystalline	1740	44.7	17.3	0.291	5810	3032

Fig. 1 **a** Schematic of the hcp crystal showing directions of the $[0001]$ and $[10\bar{1}0]$ poles. The figure on the *right* shows the extrusion and the radial directions for the commercial pure magnesium rod from which the samples were machined. The $[0001]$ poles are parallel to the radial direction while the $[10\bar{1}0]$ poles are parallel to the extrusion direction. Specimens were machined from the magnesium rod with the impact face normal to the extrusion direction. **b** EBSD grain orientation map (GOM) along the *ED* (i.e. normal to the impact surface) of the as-received magnesium samples. The weighted average grain size is $\sim 77\ \mu\text{m}$. **c** $[0001]$ an $[10\bar{1}0]$ pole figures (PF) of the as-received magnesium along the *ED* (i.e. normal to the impact surface). The figure shows that the basal poles are aligned with *RD*



the fabrication of heat-resistant optical diagnostic techniques for the measurement of the free surface particle velocity motion during the experiments; third, the elevated temperature target plates add a limitation on the stress-states that can be imparted on the sample in certain experimental configurations, which involve sandwiched specimens between hard elastic target plates because of possible thermal softening of heated target plates that must remain elastic during impact

to allow unambiguous interpretation of the experimental results from the measured particle velocity measurements; and lastly, differential thermal expansion, particularly for targets that utilize an optical window, is a perpetual issue in elevated temperature plate impact experiments, since precise tolerances between the sample, bond layer, coating(s), and window are difficult to maintain over large temperature ranges.

Fig. 2 a EBSD grain orientation map (GOM) along the ED (i.e. normal to the impact surface) of the thermally annealed magnesium sample at 600 °C for 30 min. The weighted average grain size is ~547 μm, which is much larger when compared to the as-received magnesium samples. **b** [0001] and [10 $\bar{1}$ 0] pole figures (PF) of the annealed magnesium along the ED. The figures show the basal poles reorient closer towards the ED after the thermal annealing process

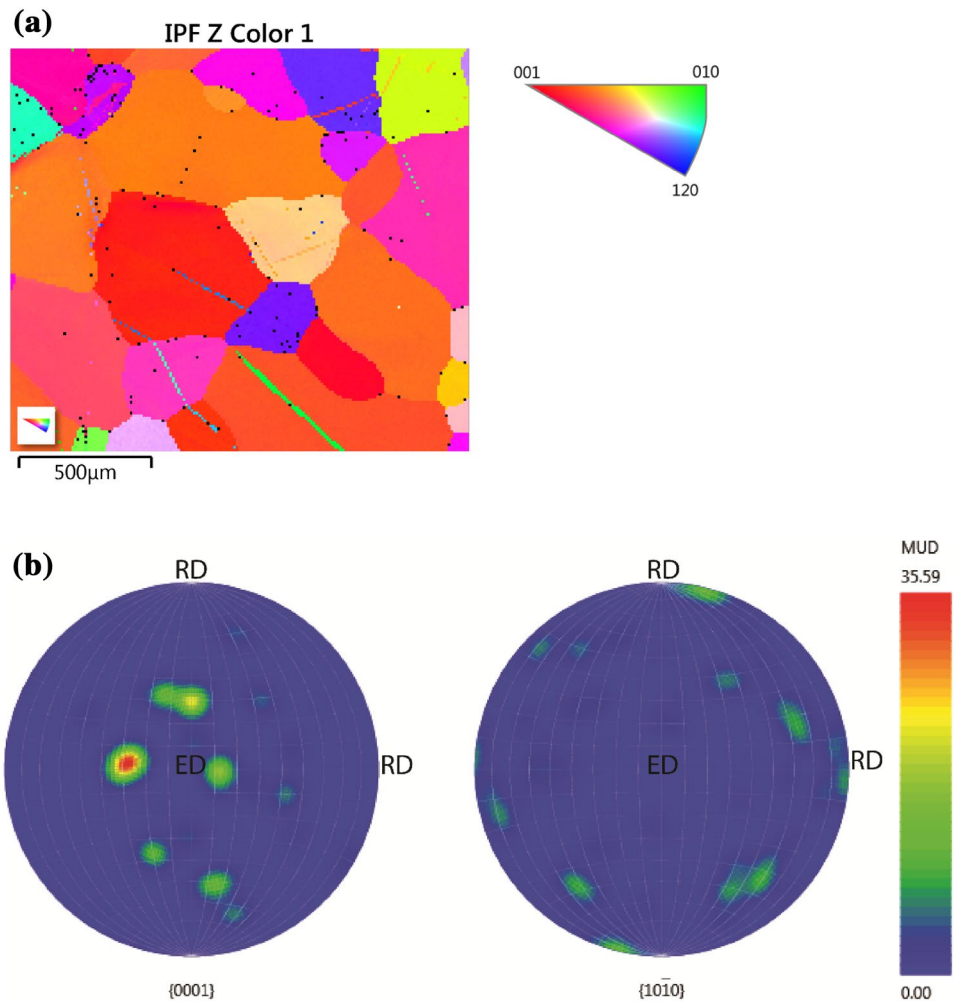


Table 2 Select physical properties of Inconel 718 alloy from High Temp Metals Inc

Material	Density (Kg/m ³)	Elastic modulus (GPa)	Shear modulus (GPa)	Poisson's ratio	Longitudinal wave speed (m/s)	Shear wave speed (m/s)
Inconel 718	8260	208	80	0.3	5820	3112

To alleviate these experimental challenges, critical modifications to the single-stage gas-gun at CWRU [2, 22] were made. In this regards, our recent analyses have shown that heating the flyer plate carried by the sabot at the breech end of the gun barrel is more attractive when compared to heating the target assembly at the exit (impact chamber) end of the gun barrel while conducting the elevated temperature plate impact experiments. By doing so, experimental challenges related to optical probe/diagnostics being too close to the heated target assembly as well as the possible loss of alignment between the target and flyer plates due to differential heating of the various sub-elements of the target holder, are minimized. Moreover, at room temperatures, the target plates are expected to remain elastic for a larger

impact velocity range, thus enabling interpretation of the experimental measurements using one dimensional elastic stress-wave theory.

The experimental configuration used in the present study is shown schematically in Fig. 3. To ensure the generation of plane-waves with a wave front sufficiently parallel to the impact face, the flyer and target plates are aligned to be parallel to within 5×10^{-4} radians by using an optical alignment scheme [23]. The actual tilt between the flyer and target plates at impact was measured by those six voltage-biased copper pins secured in the slots on the aluminum ring, which also provide the diagnostic triggering to the oscilloscopes for data recording [24]. Prior to the acceleration of the sabot, the magnesium sample (also referred to as the flyer plate) is

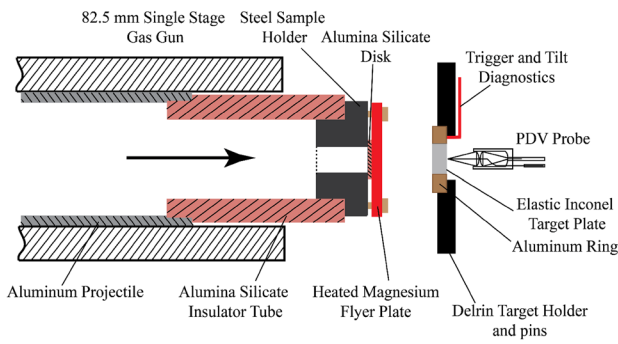


Fig. 3 Schematic of the elevated temperature normal plate impact experimental configuration used in the present study. The sabot carries the pre-heated flyer plate representing the magnesium sample, which impacts an Inconel 718 target plate. The particle velocity at the free (rear) surface of the target plate is measured by using a PDV probe [22]

heated to the desired temperature by thermal radiation using a resistive coil heater accommodated in a custom designed heater extension to the breech end of the gas gun. A sabot carrying the magnesium sample (flyer plate) is accelerated down the gun barrel by compressed nitrogen gas and is made to impact the precipitation-hardened Inconel 718 plate target. The experimental approach has been reported in detail in our previous work [2]. The impact velocity is measured utilizing a laser based velocity system and a high-frequency photodiode. To minimize the effects of oxidation of the magnesium during the sample heating phase, and also to reduce the effects of air cushion between the flyer and target plates, the target and the breech end of the gas gun are evacuated to a pressure less than 100 mTorr.

An IPG Photonics 2W Erbium fiber coupled laser with the wavelength of 1550 nm was used to provide the linearly polarized light to an in-house built custom fiber optics-based heterodyne combined NDI/TDI [22] for measuring the normal particle displacement at the rear surface of the target plate. The particle velocity versus time profile is obtained by numerical differentiation of the measured displacement with respect to time history using an in-house developed data analysis program in conjunction with the commercial package MATLAB.

Estimation of Dynamic Material Stress at the Flyer (Pre-Heated Sample)-Target Interface

For a typical normal shock compression plate-impact experiment in which a pre-heated flyer can undergo elastic–plastic deformation at the flyer-target interface at impact, the loci of all stress and particle velocity states for the target are represented by the line passing through the origin. Consequently, the stress in the target plate can be expressed as

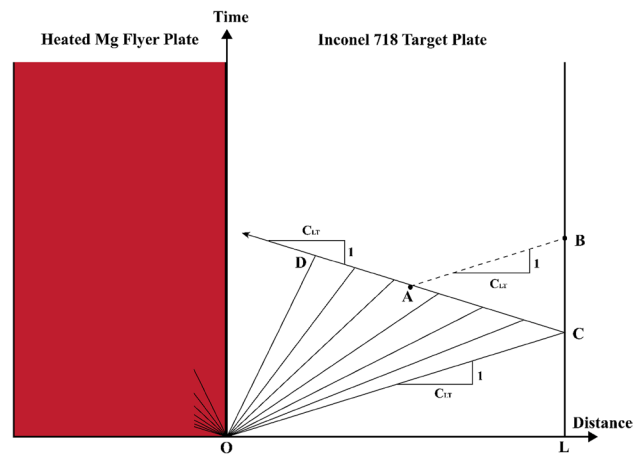


Fig. 4 Time-distance diagram for simple wave traveling into the Inconel 718 target plate with elastic unloading. C_{LT} is the elastic longitudinal wave speed of the Inconel target, A is an arbitrary point on the simple wave side of the unloading wave CD, and B is the corresponding point at which the characteristic passing through A intersects the free surface ($X=L$)

$$\sigma_T(t) = \rho_{0T} U_{sT} v_{pT}(t) \tag{1}$$

where ρ_{0T} and U_{sT} represent the mass density and shock wave speed of the Inconel 718 target plate, respectively, $(\rho_{0T} U_{sT})$ is the longitudinal impedance of the target plate, and $v_{pT}(t)$ is the history of the particle velocity in the target plate at the flyer/target interface.

Similarly, the stress in the flyer plate can be expressed as

$$\sigma_F(t) = \rho_{0F} U_{sF} (V_0 - v_{pF}(t)) \tag{2}$$

where $\rho_{0F} U_{sF}$ is the impedance of the flyer plate, ρ_{0F} and U_{sF} represent the mass density and shock wave speed of the flyer (magnesium samples), respectively, $v_{pF}(t)$ is the history of the particle velocity in the flyer plate at the flyer/target interface, and V_0 is the impact velocity.

In the analysis of the present experiments, the simple wave, strain-rate independent, longitudinal plastic wave analysis of Bodner and Clifton [25] is used to relate the free-surface velocities to the compressive stress at the flyer/target interface. Figure 4 shows a simple wave traveling into the target plate with elastic unloading. Following Clifton and Bodner [25],

$$\sigma_T(A) + \rho_{0T} C_{LT} v_{pT}(A) = \rho_{0T} C_{LT} v_{pT}(B) \tag{3}$$

where σ_T is the compressive stress in the target, C_{LT} is the elastic longitudinal wave speed of the Inconel target, A is an arbitrary point on the simple wave side of the unloading wave CD, and B is the corresponding point at which the characteristic passing through A intersects the free surface ($X=L$). The relation between particle velocity and stress at any interior point in the target is given by [25]

$$v_{pT} = \Phi(\sigma_T) = \int_0^{\sigma_T} \frac{d\sigma_T}{\rho_{0T} U_{sT}(\sigma_T)} \tag{4}$$

where, $U_{sT}(\sigma_T)$ is the longitudinal wave speed through material under a normal stress σ_T .

For an Inconel 718 target with a stress–strain curve that is concave towards the strain axis, the wave speed $U_{sT}(\sigma_T)$ decreases monotonically with increasing σ_T . Substituting Eq. (4) into Eq. (3) and taking differentials, one obtains

$$d\sigma_T(A) = \frac{\rho_{0T} C_{LT} U_{sT}(\sigma_T(A))}{U_{sT}(\sigma_T(A)) + C_{LT}} dv_{pT}(B) \tag{5}$$

Equation (5) can be integrated by taking the point after point C to be discretized into equal intervals $h = 1/f$, where $f = 2.5 \times 10^{10}$ is the sampling rate of the digital oscilloscope. Denoting $t = nh$ by t^n , point B = (L, L/C_{LT} + tⁿ) by Bⁿ, and the corresponding point A by Aⁿ, we can introduce the notation $\sigma_T^n = \sigma_T(A^n)$; $v_{pT}^n = v_{pT}(B^n)$; $U_{sT}^n = U_{sT}(\sigma_T^n)$; and $\Phi^n = \Phi(\sigma_T(A^n))$. Using the average value for $1/U_{sT}(\sigma_T)$ over a typical time interval, i.e. over t^{n-1} and t^n , we can write

$$\sigma_T^n = \sigma_T^{n-1} + \frac{\rho_{0T} C_{LT} \left[\frac{v_{pT}^n - v_{pT}^{n-1}}{\rho_T} \right]}{1 + \frac{C_{LT}}{2} \left[\frac{1}{U_{sT}^n} + \frac{1}{U_{sT}^{n-1}} \right]} \tag{6}$$

The wave velocity U_{sT}^n can be deduced from the characteristics travelling through Aⁿ:

$$U_{sT}^n = \left[\frac{\frac{L}{C_{LT}} - \frac{t^n}{2}}{\frac{L}{C_{LT}} + \frac{t^n}{2}} \right] C_{LT} \tag{7}$$

where L is the thickness of the target plate.

To compute the strain ϵ^n at (Aⁿ), Eq. (4) can be rewritten in terms of strain as

$$v_{pT} = \int_0^{\epsilon} U_{sT}(\epsilon) d\epsilon \tag{8}$$

Integrating Eq. (8) over the time interval t^{n-1} to t^n yields,

$$\epsilon^n = \epsilon^{n-1} + \frac{\left[\frac{v_{pT}^n - v_{pT}^{n-1}}{\rho_T} \right]}{\left[U_{sT}^n + U_{sT}^{n-1} \right]} \tag{9}$$

Figure 5 shows the stress versus strain curve obtained by using Eq. (1–9) for a symmetric impact test on Inconel 718 alloy, which represents the target plate material in the present experiments. The thickness of the target plate is 7.145 mm. The impact velocity used in the experiment is ~149 m/s. The solid red line shows the calculated stress versus strain curve from the experimental free surface particle velocity data, whereas that dashed line represents a line with a slope equal to $(1 - \nu)E / (1 + \nu)(1 - 2\nu)$, where

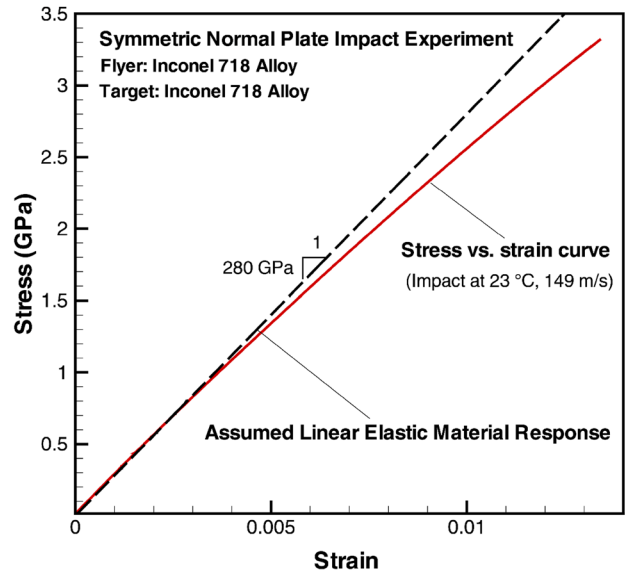


Fig. 5 Stress versus strain curve for symmetric impact test on Inconel 718 alloy at 23 °C, the impact velocity is ~149 m/s. The slope of the dashed line is equal to $(1 - \nu)E / (1 + \nu)(1 - 2\nu)$, where ν and E are Poisson’s Ratio and the elastic modulus of the Inconel 718 target, respectively. Small deviations from linear behavior are observed above a compressive stress of ~0.75 GPa

ν and E are Poisson’s ratio and the elastic modulus of the Inconel 718 target, respectively. Small deviations from linear behavior are observed above a compressive stress level of ~0.75 GPa. Since the measured yield strength of Inconel 718 are of the same order as the applied stress levels used in the present experiments, longitudinal elastic wave speed C_{LT} is replaced by the inelastic, stress-dependent wave speed of the Inconel target U_{sT} , to estimate the dynamic stress and particle velocity history at the flyer/target interface from the measured free surface particle velocity profiles. Consequently, using Eq. (1), the dynamic material stress, $\sigma_F(t)$, in the heated magnesium sample at the target-flyer interface can be estimated at conditions of incipient plasticity and post yield in terms of the free-surface particle velocity $v_{fs}(t)$, as [26, 27].

$$\sigma_T(t) = \sigma_F(t) = \rho_{0T} U_{sT} \left[\frac{1}{1 + \frac{U_{sT}}{C_{LT}}} \right] v_{fs}(t) \tag{10}$$

An average value for U_{sT} is estimated as 5769 m/s from the symmetric impact experiment on Inconel 718. It is to be noted that even though post impact the magnesium sample (flyer) is expected to become highly anisotropic during impact, the use of Eq. (10) to estimate the dynamic stress in the Mg sample at the flyer-target interface at the onset of incipient plasticity and post yield, only involves the knowledge of the room temperature impedance in the

direction of impact and the free surface particle velocity measurements in the isotropic Inconel 718 target plate.

Experimental Results and Discussion

In the present study, a series of seven normal plate impact experiments are conducted on commercial purity (99.9%) polycrystalline magnesium samples at test temperatures in the range from room to near melt (~ 630 °C) under dynamic uniaxial strain shock compression. These experiments are conducted to gain insights into the temperature dependence of dynamic material stress of magnesium at incipient plasticity. The experimental conditions (e.g. flyer and target plate thickness, impact velocities, the angle of flyer-target misalignment (tilt) at impact and initial sample temperatures) for each experiment are summarized in Table 3. As noted from the table, the impact velocities used in the experiments lie in the narrow range of 100 to 110 m/s, which are sufficient to take the Mg samples to their inelastic (elastic–plastic) deformation regime at the target-flyer (sample) interface at impact.

Shock Response of Commercial Purity 99.9% Polycrystalline Magnesium at Elevated Test Temperatures

As mentioned in “[Experimental Work](#)”, the velocity history at the free surface of the target can be used to determine the dynamic stress at the flyer/target interface at incipient plasticity and subsequent plastic flow. If one focuses on the initial rise (wavefront) of the particle velocity profiles shown in Fig. 6, three distinctive regions can be observed—an initial sharp rise, followed by a less steep rise region, which eventually reaches a plateau. The initial linear rise in the particle velocity profile is controlled by the elastic behavior of the flyer and target materials, while the subsequent ramp region provides information on the dynamic stress in the magnesium samples at the interface of the target/flyer plates at onset of plasticity and post-yield. These profiles indicate progressively lower levels of dynamic

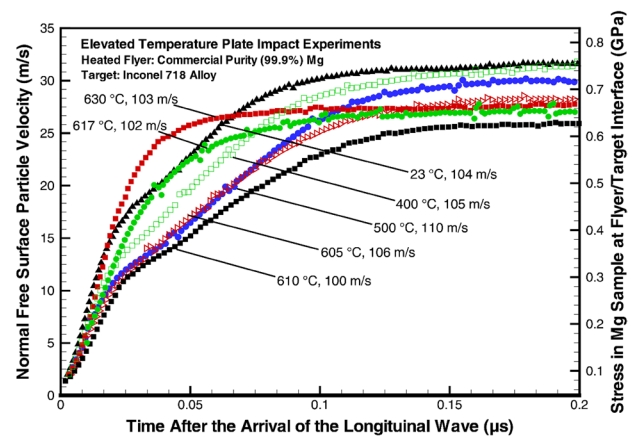


Fig. 6 The onset of incipient plasticity in commercial purity 99.9% polycrystalline magnesium samples in the temperature range 23–630 °C. Progressively lower dynamic stresses with increasing sample temperatures were observed. However, the rate of thermal softening is observed to weaken at test temperatures from 500 to 610 °C; this trend found to even reverse itself at 617 and 630 °C, where strengthening effects overtake the thermal softening

material stress (strength) for the shock loaded magnesium as the test temperatures are increased from room to 500 °C. A distinct knee in the free-surface particle velocity profile is observed at the transition from the initial nearly linear rise to a more gradual rise in particle velocity. This knee corresponds to a stress level ~ 320 MPa for the room temperature experiment, and then decreases to ~ 290 MPa as the test temperature is increased to 400 °C. Further softening in stress to ~ 240 MPa is observed at the test temperature of 500 °C. At sample temperatures in the range 500–610 °C, however, there is no apparent net change in the dynamic material stress, indicating that other dynamic strengthening mechanisms come into play that compete with thermal softening. The dynamic yield stress in this temperature range is ~ 240 MPa. At still higher test temperatures, approaching the melt point of magnesium (617 and 630 °C), a clear reversal in this trend occurs with a distinct increase in the dynamic material stress when compared to those observed at test temperatures in the range 23–610 °C. The free surface

Table 3 Summary of the elevated temperature normal plate impact experiments conducted in the present study on commercial purity magnesium

Experiment no.	Flyer thickness (mm)	Target thickness (mm)	Impact velocity (m/s)	Tilt at impact (mrad)	Initial sample temperature (°C)
1	5.9	7.2	104 ± 2	0.56	23 ± 1
2	5.9	7.2	105 ± 2	0.84	400 ± 1
3	5.9	7.1	110 ± 2	1.33	500 ± 1
4	5.9	7.2	106 ± 2	0.42	605 ± 1
5	5.8	7.2	100 ± 2	0.88	610 ± 1
6	5.9	7.1	102 ± 2	0.65	617 ± 1
7	5.8	7.1	103 ± 2	1.40	630 ± 1

particle velocity at the wave-front, in the two highest temperature experiments is observed to increase nearly linearly before reaching a plateau.

This dramatic increase in particle velocity is understood to be indicative of a transition in plastic deformation mechanism for magnesium from thermal activation at temperatures in the range from room to 610 °C. For example, in the recent past, a modest increase in testing temperature has also been shown to affect the shock response of Mg, primarily the elastic precursor [28]. For instance, large increases in the elastic precursor were observed at temperatures approaching the sample melting point. This was also seen in aluminum [29]. This was attributed to the Frenkel disorder [29], i.e. spontaneous nucleation of point defects at the elevated temperatures from their normal lattice positions to interstitial positions. Theoretically, the end result is increased resistance to activation and motion of dislocations. However, it

is not clear that this process would occur quickly enough to result in the observed strengthening in magnesium during shock loading. Similar behavior has also been reported in heated single crystals of aluminum where the cause of the strength increase was attributed to phonon drag on dislocations [30]. This transition in plastic flow mechanism to viscous (phonon) drag near melt temperatures leading to net dynamic material strengthening has also been reported for pure cobalt (hcp phase) at elevated temperatures under planar impact at strain-rates $\sim 10^5\text{--}10^6/\text{s}$ [15]. A comprehensive insight into the contribution of the microstructural evolution to the dynamic response observed in the present experiments is currently being investigated and will be reported in future publications.

Next, focusing attention to the plateau region of the measured free surface particle velocity profiles in Fig. 7, it is observed that the levels of particle velocities decrease continuously as the sample test temperatures are increased from room to 610 °C. As the sample temperatures are increased, the decreasing trend in particle velocity is reversed and the particle velocity is observed to increase at test temperatures of 617 and 630 °C. It is to be noted that the free surface particle velocity profiles can be related to the plastic impedance of the flyer plate at various sample temperatures employed in the present experiments. By equating Eqs. (1) and (2), the magnitude of the plastic impedance of the flyer (sample) can be related to the measured free surface particle velocity, the impact velocity, physical properties of the flyer and target plates, and the known impedance of the target plate:

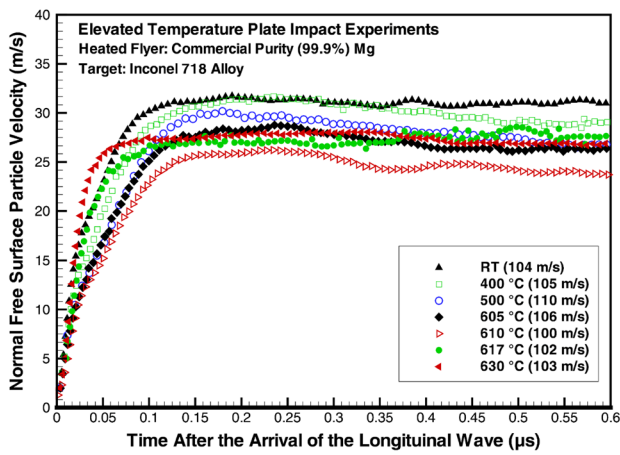


Fig. 7 Shock response of commercial purity 99.9% polycrystalline magnesium samples in the temperature range 23–630 °C. The experiments were conducted in a narrow impact velocity range of $\sim 100\text{--}110$ m/s. It is observed that the levels of particle velocities decrease continuously as the sample test temperatures are increased from room to 610 °C; as the sample temperatures are increased the decrease in particle velocity trend is reversed and the free-surface particle velocity increases at test temperatures of 617 and 630 °C

$$\rho_{0F}U_{sF} = \frac{\rho_{0T}U_{sT}v_{pT}(t)}{[V_o - v_{pF}(t)]} \tag{11}$$

Recall that at the impact interface

$$v_{pF}(t) = v_{pT}(t) = \frac{1}{\left[1 + \frac{U_{sT}}{C_{LT}}\right]} v_{fs}(t) \tag{12}$$

Table 4 Plastic impedance of the commercial purity 99.9% magnesium samples for seven experiments

Experiment No.	Sample temperature (°C)	Impact velocity (m/s)	Average free-surface velocity at plateau (m/s)	Plastic impedance of magnesium flyer (kg/m ² s)
1	23	104	31.10	7312862
2	400	105	30.08	6945948
3	500	110	28.06	6306797
4	605	106	27.81	6256386
5	610	100	24.78	5851555
6	617	102	27.38	6413393
7	630	103	27.40	6417704

Average values for shock wave speed U_{sT} of the Inconel target plate and free-surface velocities v_{fs} at plateau are estimated from the particle velocity profile for each experiment.

Based on Eqs. (11) and (12), the plastic impedance of magnesium flyer (sample) $\rho_{0F}U_{sF}$, at different test temperatures are estimated, and summarized in Table 4. As noted from the table, the longitudinal (plastic) impedance of magnesium samples decreases continuously as the sample test temperatures are increased from room to 610 °C. As the sample temperatures are increased to 617 and 630 °C, the trend is observed to decrease indicating an increase in material strength.

Estimated Strain-Rates and Strain in Shock Compressed Magnesium Sample at Elevated Temperatures

Knowledge of physical properties of magnesium, e.g. density, bulk wave speed, etc. as a function of temperature is required to estimate the strains and the strain-rates in the sample under the uniaxial strain impact loading conditions. The linear thermal expansion coefficient ϵ_T ($10^{-6}/^\circ\text{C}$) of commercially pure polycrystalline magnesium at any temperature T (°C) is described by the relationship $\epsilon_T = 24.66 + 0.01952T$ [31]; this relationship can be used to estimate the density of shock loaded magnesium, ρ_{0F} , at various test temperatures. The molar heat capacity of magnesium C_p (J/K/mole) as a function of temperature T (°C) can be described, within sufficient accuracy, by the relationship $C_p = 24.5337208 + 1.0704764 \times 10^{-2}T - 0.4803232 \times 10^{-8}T^2$ [32]. Since the measurement of the plastic wave arrival times cannot be made within the test window of the present reverse geometry plate impact experiments, the plastic wave speeds of magnesium flyer, U_{sF} , in the direction of impact can be estimated using [33]

$$U_{sF} = C_b + 1.26v_{fs} \tag{13}$$

where C_b is the bulk wave speed of magnesium samples at zero pressure, defined as $\sqrt{K/\rho_{0F}}$, where K represents the Voigt average bulk modulus of the sample [34]. The Voigt

average bulk modulus of hcp magnesium can be expressed using the temperature dependent elastic constants C_{11} , C_{33} , C_{12} and C_{13} as

$$K = \frac{(2C_{11}+C_{33}+2C_{12}+4C_{13})}{9} \tag{14}$$

with the bulk wave speed given by the relationship

$$C_b = \sqrt{(2C_{11} + C_{33} + 2C_{12} + 4C_{13})/9\rho_{0F}} \tag{15}$$

The temperature dependent elastic constants for magnesium in Eq. (15) can be obtained from the experimental data provided in [35] at 27 °C, combined with estimates for dC_{ij}/dT provided in [36]:

$$C_{11} = 59.40 - 0.024 (T - 27) \text{ GPa} \tag{16}$$

$$C_{33} = 61.60 - 0.026 (T - 27) \text{ GPa} \tag{17}$$

$$C_{12} = 25.61 - 0.005 (T - 27) \text{ GPa} \tag{18}$$

$$C_{13} = 21.44 \text{ GPa} \tag{19}$$

The important physical properties for commercial purity magnesium are listed in Table 5.

To estimate the strain-rate and strain histories in the impact loaded magnesium samples in the present experiments, the speed of plastic wave propagation in the sample, U_{sF} is expressed as

$$U_{sF} = \sqrt{\frac{d\sigma_F/d\epsilon_F}{\rho_{0F}}} \tag{20}$$

where, ρ_{0F} , represents the mass density of magnesium sample (flyer), σ_F and ϵ_F represent the stress and strain in magnesium sample, respectively. Note, because of the use of reverse plate impact geometry used in the present study, the plastic wave speeds of magnesium samples cannot be directly obtained from the measurements of the free surface particle velocity profiles on the target plate.

Manipulating Eqs. (10) and (20), yields

$$d\epsilon_F(t) = \frac{1}{1+U_{sT}/C_{LT}} \frac{1}{U_{sF}} dv_{fs}(t) \tag{21}$$

Table 5 Select physical and thermal properties for the commercial purity 99.9% magnesium samples as a function of temperature

Sample temperature (°C)	Density (kg/m ³)	Bulk wave speed (m/s)	Linear thermal expansion coefficient (10 ⁻⁶ /°C)	Molar heat capacity (J/K/mole)
23	1740	4504	25.109	24.78
400	1678	4356	32.468	28.815
500	1657	4318	34.42	29.885
605	1634	4278	36.47	31.008
610	1633	4276	36.567	31.062
617	1631	4274	36.704	31.137
630	1628	4269	36.958	31.276

and

$$\dot{\epsilon}_F(t) = \frac{1}{1+U_{sT}/C_{LT}} \frac{1}{U_{sF}} \dot{v}_{fs} \quad (22)$$

Consequently, Eqs. (21) and (22) can be used to provide estimates for strain and strain-rates in the magnesium samples. Analysis performed on the all seven data sets shows comparable strain-rate levels in the range of 6×10^4 – 1.3×10^5 /s.

The dynamic yield stress at the “knee” for the experiment at room temperature (~320 MPa) is comparable to the previously reported value at the HEL (~390 MPa) for high purity (99.999%) magnesium single crystal shock loaded along [10 $\bar{1}$ 0] orientation at similar strain-rates on the order of 10^5 /s [14].

Estimated Temperature Rise in Magnesium Sample due to Plastic Work to Heat Conversion During High Strain Rate Deformation

The temperature of magnesium sample subjected to dynamic loading can be increased by the conversion of the dynamic plastic work into heat during the high strain-rate deformation of the magnesium sample. The heat capacity of magnesium is assumed to be constant over the pressures of interest in the present experiments, but dependent on sample temperature [32, 37]. The upper bound of the temperature rise in magnesium sample is obtained using a common assumption of $\beta=0.9$ (the ratio of plastic work to heat conversion), even though considerably smaller factor for pure magnesium has been reported [38], and by assuming an adiabatic deformation process. Also, the melting temperature of magnesium is assumed to increase proportionally with pressure [39]. The melting temperature and sample temperature profiles for shock loaded magnesium, for the case of Experiments 4 and 7, are shown in Fig. 8. Both the melt and sample temperatures are observed to increase after impact. However, the melt temperatures increase at a much faster rate when compared to the sample temperatures. This trend can be observed from the dotted lines, which show the ratio of the instantaneous sample temperature to the instantaneous melt temperature (T_s/T_m). This ratio, in both experiments, decreases as the sample is shock loaded, indicating that the sample temperatures diverge from the corresponding melt temperatures with time after impact. Also, the result shows a sharper initial increase in melt temperatures for Experiment No. 7, which is in a good agreement with the fact that the dynamic stress of magnesium in this experiment increases to a higher level within a shorter time. Following the initial rise, the melt and sample temperatures both reach a plateau and remain nearly constant thereafter.

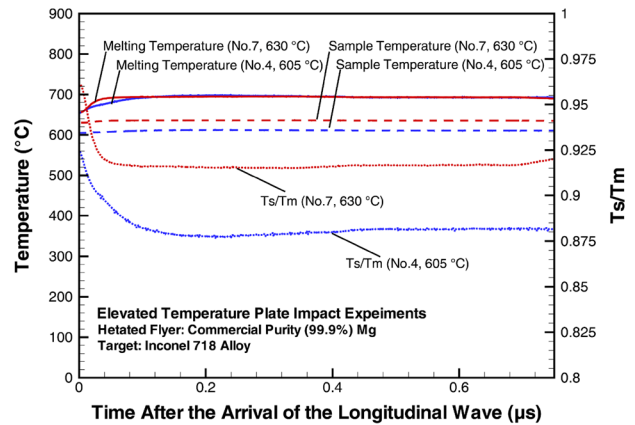


Fig. 8 Plots showing the sample temperature T_s in the magnesium sample as a function of time after impact due to the adiabatic conversion of plastic work to heat for select experiments (Experiments Nos. 4 and 7), along with the pressure dependent melting temperature, T_m . The ratio of T_s/T_m (shown by the dotted lines) reveal that the sample temperatures diverge from their corresponding melt temperatures even for the case of the highest test temperature (630 °C) experiment

Potential Effects of Grain Coarsening and Crystal Reorientation on the Macroscopic Response of Shock Compressed Magnesium

The microstructural evolution of magnesium during the sample heating process, as inferred from the EBSD analysis, is noteworthy. The pre-test sample heating (annealing) is observed to result in both grain coarsening as well as crystal reorientation due to recrystallization in the samples. The former is understood to be important in controlling the mechanical response of magnesium, since grain boundaries are understood to act as the obstacles to dislocation motion due to the discontinuity in slip planes caused by lattice mismatch at the grain boundaries. When the grain size is relatively large, higher stress concentration can occur at the boundary of adjacent grains due to increased dislocation pile-up at the grain boundaries, which can act as a driving force to prompt dislocation motion. So, it is plausible to expect the material with larger grain size (i.e. more intense dislocation pile-up) to exhibit lower strengths when compared to samples with smaller grain size. Also, a decrease in strength of magnesium (grain size over $\sim 1 \mu\text{m}$) with increasing grain size at quasi-strain rates and room temperature is predicted by the Hall–Petch relationship [40, 41]. Aside from the effect of grain size, the texture of magnesium sample relative to the loading direction can have a significant influence on its mechanical properties because of the anisotropic hcp crystal structure [14, 42]. From the GOM and PF in Fig. 2, the basal poles are observed to reorient closer towards the extrusion direction (ED) after annealing, with the c-axis of the majority of the grains in the annealed sample at $\sim 30^\circ$ with respect to the extrusion direction. Therefore, depending

on the sample temperature, different deformation modes can be activated within the magnesium samples, which could possibly contribute to either material softening or hardening. Further investigation is underway to better understand the role of microstructural features including texture development in the observed macroscopic softening/strengthening response of magnesium, and will be reported in subsequent manuscripts by the authors.

Summary

In the present study, temperature dependence of the dynamic yield stress under uniaxial strain compression and the dynamic flow stress post yield of commercial purity 99.9% polycrystalline magnesium have been investigated in a series of normal plate impact experiments conducted at strain rates $\sim 10^5/s$ and temperatures in the range 23–630 °C. A progressive softening in dynamic stress with increasing test temperatures is observed in the temperature range 23–500 °C. At higher temperatures ranging from 500 to 610 °C, no apparent net increase of dynamic stress is observed. At still higher test temperatures (617 and 630 °C), a dramatic increase in net dynamic stress is observed. EBSD analysis of the as-received and annealed pre-test magnesium samples reveal grain coarsening as well as grain re-orientation during the heating process of the samples. Since the basal poles are aligned along the RD for the as-received samples, non-basal slip and twinning are expected as the dominant deformation modes, leading to a higher critical stress to initiate the plastic flow when compared to primary basal slip. As the test temperatures are increased, crystallographic texture can possibly evolve to be more favorable for basal slip as shown in Fig. 2b; this along with the significant level of grain coarsening, could likely contribute to soften the magnesium as the test temperatures are increased. The progressive softening observed at temperatures in the range 23–500 °C is believed to be controlled by the thermal activation mechanism. However, at test temperatures in the range 500–610 °C, there is no apparent net change in the dynamic stress, which is contrary to the assumption of thermal activation being the dominant deformation mechanism. At even higher test temperatures, approaching the melt point of magnesium (617 and 630 °C), a clear reversal in this trend is observed which manifests itself as an increase in the free surface particle velocity at yield and post-yield, and is understood to be as a result of increasing dynamic yield stress of the material. Moreover, the measured free surface particle velocity post-yield for the 630 °C test temperature experiment is higher than those measured in experiments at lower test temperatures. These observations suggest that at high strain-rates and elevated test temperatures employed in the present study, dynamic strengthening/softening mechanisms other than

thermal activation of dislocations past obstacles are playing a dominant role in controlling the dynamic strength of polycrystalline magnesium. These strengthening effects could be attributed to either phonon viscous drag acting on dislocations at high strain rates and elevated temperatures and/or Frenkel disorder [29], which can lead to spontaneous nucleation of point defects at elevated temperatures, and consequently increased resistance to activation and motion of dislocations. A comprehensive insight into the contribution of the microstructural evolution to the dynamic response observed in the present experiments is currently being investigated and will be reported in future publications.

Acknowledgements The authors would like to acknowledge the financial support of the U.S. Department of Energy through the Stewardship Science Academic Alliance (Grant Nos. DE-NA0001989 and DE-NA0002919) in conducting the present research. The authors would also express gratitude to Swagelok Center for Surface Analysis of Materials (SCSAM) at CWRU for the EBSD data.

References

1. Ramesh K (2002) Effects of high rates of loading on the deformation behavior and failure mechanisms of hexagonal close-packed metals and alloys. *Metall Mater Trans A* 33(3):927–935
2. Zuanetti B, Wang T, Prakash V (2017) A novel approach for plate impact experiments to determine the dynamic behavior of materials under extreme conditions. *J Dyn Behav Mater* 3(1):64–75
3. Mises RV (1928) Mechanik der plastischen formänderung von kristallen. *ZAMM J Appl Math Mech* 8(3):161–185
4. Groves G, Kelly A (1963) Independent slip systems in crystals. *Philos Mag* 8(89):877–887
5. Berge F, Krüger L, Ouaziz H, Ullrich C (2015) Influence of temperature and strain rate on flow stress behavior of twin-roll cast, rolled and heat-treated AZ31 magnesium alloys. *Trans Nonferrous Met Soc China* 25(1):1–13
6. Wonsiewicz B, Backofen W (1967) Independent slip systems and ductility of hexagonal polycrystals. *Trans Metall Soc AIME* 239:1422–1433
7. Kumar A, Hauser F, Dorn J (1968) Viscous drag on dislocations in aluminum at high strain rates. *Acta Metall* 16(9):1189–1197
8. Regazzoni G, Kocks U, Follansbee PS (1987) Dislocation kinetics at high strain rates. *Acta Metall* 35(12):2865–2875
9. Li Q (2011) Dynamic mechanical response of magnesium single crystal under compression loading: experiments, model, and simulations. *J Appl Phys* 109(10):103514
10. Dixit N (2015) A mechanism based investigation of the dynamic behavior of pure magnesium. Dissertation, Johns Hopkins University, Baltimore, MD
11. Prasad KE, Li B, Dixit N, Shaffer M, Mathaudhu S, Ramesh K (2014) The dynamic flow and failure behavior of magnesium and magnesium alloys. *JOM* 66(2):291–304
12. Yoshinaga H, Horiuchi R (1964) On the nonbasal slip in magnesium crystals. *Trans Jpn Inst Met* 5(1):14–21
13. Al-Samman T, Molodov KD, Molodov DA, Gottstein G, Suwas S (2012) Softening and dynamic recrystallization in magnesium single crystals during c-axis compression. *Acta Mater* 60(2):537–545
14. Kanel G, Garkushin G, Savinykh A, Razorenov S, de Resseguier T, Proud W, Tyutin M (2014) Shock response of magnesium

- single crystals at normal and elevated temperatures. *J Appl Phys* 116(14):143504
15. Zaretsky E (2010) Impact response of cobalt over the 300–1400 K temperature range. *J Appl Phys* 108(8):083525
 16. Prakash V, Clifton RJ (1990) Experimental and analytical investigation of dynamic fracture under conditions of plane strain. In: Ernst HA, Saxena A, McDowell DL (Eds.) *Fracture mechanics: twenty-second symposium, Vol. 1*, American Society for Testing, Philadelphia, pp 412–444
 17. Liou NS, Okada M, Prakash V (2004) Formation of molten metal films during metal-on-metal slip under extreme interfacial conditions. *J Mech Phys Solids* 52(9):2025–2056
 18. Yuan F, Liou N-S, Prakash V (2009) High-speed frictional slip at metal-on-metal interfaces. *Int J Plast* 25(4):612–634. doi:10.1016/j.ijplas.2008.12.006
 19. Yuan F, Tsai L, Prakash V, Rajendran A, Dandekar D (2007) Spall strength of glass fiber reinforced polymer composites. *Int J Solids Struct* 44(24):7731–7747. doi:10.1016/j.ijsolstr.2007.05.007
 20. Tsai L, Prakash V (2005) Structure of weak shock waves in 2-D layered material systems. *Int J Solids Struct* 42(2):727–750
 21. Fruttschy KJ, Clifton RJ (1998) High-temperature pressure-shear plate impact experiments using pure tungsten carbide impactors. *Exp Mech* 38(2):116–125
 22. Zuanetti B, Wang T, Prakash V (2017) A compact fiber optics-based heterodyne combined normal and transverse displacement interferometer. *Rev Sci Instrum* 88(3):033108
 23. Kumar P, Clifton R (1977) Optical alignment of impact faces for plate impact experiments. *J Appl Phys* 48(3):1366–1367
 24. Prakash V (1998) Time-resolved friction with applications to high-speed machining: experimental observations. *Tribol Trans* 41(2):189–198
 25. Clifton R, Bodner SR (1966) An analysis of longitudinal elastic-plastic pulse propagation. *J Appl Mech* 33(2):248–255
 26. Okada M, Liou N-S, Prakash V, Miyoshi K (2001) Tribology of high-speed metal-on-metal sliding at near-melt and fully-melt interfacial temperatures. *Wear* 249(8):672–686
 27. Prakash V, Mehta N (2012) Uniaxial compression and combined compression-and-shear response of amorphous polycarbonate at high loading rates. *Polym Eng Sci* 52(6):1217–1231
 28. Yoo M (1981) Slip, twinning, and fracture in hexagonal close-packed metals. *Metall Trans A* 12(3):409–418
 29. Frenkel J (1926) Über die Wärmebewegung in festen und flüssigen Körpern. *Zeitschrift für Physik* 35(8–9):652–669
 30. Kanel G, Razorenov S, Baumung K, Singer J (2001) Dynamic yield and tensile strength of aluminum single crystals at temperatures up to the melting point. *J Appl Phys* 90(1):136–143
 31. Hidnert P, Sweeney W (1928) Thermal expansion of magnesium and some of its alloys. *Bur Stand Jour Res* 1(5):771–792
 32. Poppema T, Jaeger F (1935) The exact measurement of the specific heats of solid substances at higher temperatures. XIX. The specific heat of zinc, magnesium, and their binary alloy, MgZn. *Proc Acad Sci Amst* 38:510
 33. Marsh SP (1980) *LASL shock Hugoniot data. Vol. 5*, University of California Press, Berkeley, CA
 34. Shazly M, Prakash V (2008) Shock response of a gamma titanium aluminide. *J Appl Phys* 104(8):083513
 35. Slutsky LJ, Garland CW (1957) Elastic constants of magnesium from 4.2 K to 300 K. *Phys Rev* 107(4):972–976
 36. Greeff C, Moriarty JA (1999) Ab initio thermoelasticity of magnesium. *Phys Rev B* 59(5):3427
 37. Grunschel SE (2009) *Pressure-shear plate impact experiments on high-purity aluminum at temperatures approaching melt*. Brown University, Providence, RI
 38. Ghosh D, Kingstedt OT, Ravichandran G (2017) Plastic work to heat conversion during high-strain rate deformation of Mg and Mg alloy. *Metall Mater Trans A* 48(1):14–19
 39. Errandonea D (2010) The melting curve of ten metals up to 12 GPa and 1600 K. *J Appl Phys* 108(3):033517
 40. Choi H, Kim Y, Shin J, Bae D (2010) Deformation behavior of magnesium in the grain size spectrum from nano-to micrometer. *Mater Sci Eng A* 527(6):1565–1570
 41. Somekawa H, Mukai T (2005) Effect of grain refinement on fracture toughness in extruded pure magnesium. *Scr Mater* 53(9):1059–1064
 42. Ulacia I, Dudamell N, Gálvez F, Yi S, Pérez-Prado M, Hurtado I (2010) Mechanical behavior and microstructural evolution of a Mg AZ31 sheet at dynamic strain rates. *Acta Mater* 58(8):2988–2998